energies

Article

Burning Behaviour of High-Pressure CH$_4$-H$_2$-Air Mixtures

Vincenzo Moccia * and Jacopo D'Alessio

CNR—Istituto Motori, Via Marconi 4, Napoli 80125, Italy; E-Mail: j.dalessio@im.cnr.it

* Author to whom correspondence should be addressed; E-Mail: v.moccia@im.cnr.it;
Tel.: +39-081-7177-124; Fax: +39-081-2396-097.

Abstract: Experimental characterization of the burning behavior of gaseous mixtures has been carried out, analyzing spherical expanding flames. Tests were performed in the Device for Hydrogen-Air Reaction Mode Analysis (DHARMA) laboratory of Istituto Motori—CNR. Based on a high-pressure, constant-volume bomb, the activity is aimed at populating a systematic database on the burning properties of CH$_4$, H$_2$ and other species of interest, in conditions typical of internal combustion (i.c.) engines and gas turbines. High-speed shadowgraph is used to record the flame growth, allowing to infer the laminar burning parameters and the flame stability properties. Mixtures of CH$_4$, H$_2$ and air have been analyzed at initial temperature 293÷305 K, initial pressure 3÷18 bar and equivalence ratio ϕ = 1.0. The amount of H$_2$ in the mixture was 0%, 20% and 30% (vol.). The effect of the initial pressure and of the Hydrogen content on the laminar burning velocity and the Markstein length has been evaluated: the relative weight and mutual interaction has been assessed of the two controlling parameters. Analysis has been carried out of the flame instability, expressed in terms of the critical radius for the onset of cellularity, as a function of the operating conditions.

Keywords: combustion; laminar burning velocity; hydrogen; methane; shadowgraph

Nomenclature:

A	flame area (mm^2)	Pe_{cr}	critical Peclet number (r_{cr}/δ_l)
Le	Lewis number	r_{cr}	critical flame radius (mm)
L_b	burned gas Markstein length (mm)	r_u	cold flame front radius (mm)
Ma	Markstein number (L_b/δ_l)	T	temperature (K)
P	pressure (bar)		

u_{l0}	unstretched laminar burning velocity (cm/s)	V_s	stretched flame speed (m/s)
		V_{s0}	unstretched flame speed (m/s)

Greek Letters

Superscripts and Subscripts

α	flame stretch rate (s^{-1})	0	initial
β	pressure index in Equation (11)	b	burned gas
γ	temperature index in Equation (11)	l	laminar
ϕ	equivalence ratio	r	reference
ρ	gas density (kg/m^3)	u	unburned gas
δ_l	laminar flame thickness (mm)		
ν	kinematic viscosity (m^2/s)		
μ	dynamic viscosity (kg/m·s)		

1. Introduction

No matter the claim and the quest for new answers to the needs of an energy-thirstier society, thermal conversion systems will play a key role in the energy supply chain. This awareness, along with the urgent need of CO_2 reduction (currently the main driver of technology advance), has at least two direct consequences: the introduction in the energy cycle of CO_2-neutral fuels (biomass-derived) and the design/development of more efficient conversion systems. The latter point can be anticipated to have a larger practical impact than the former, given the majority of energy sources will be represented by fossil fuels for many years to come.

Sometimes placed in the category of "alternative" fuels, methane (CH_4) is indeed a hydrocarbon, sporting the peculiarity of the lowest C/H ratio, if compared to other fuels: by trivial reasoning, the less the carbon, the less the CO_2. This feature has boosted a renewed attention to CH_4, which represents the main constituent of natural gas. CH_4 has been used with heat engines for a long time, even if with the status of a "niche" solution: as a fuel for internal combustion (i.c.) engines, it offers some advantages over gasoline, having wider flammable limits and better anti-knock characteristics, at the cost of a lower flame speed. A feasible opportunity to overcome the limits of CH_4 is offered by H_2: adding H_2 to CH_4 (or natural gas) can improve the flame speed/stability and lower the lean operating limit. The overall effect is to extend the stable operation map to extreme conditions (e.g., high EGR).

Crucial for the development and design of i.c. engines and gas turbine combustors is the knowledge of laminar combustion properties: they offer the basis for modelling and simulation of flame-turbulence interaction. Data on the combustion properties of pure gaseous fuels are widely available in the literature [1–12], but hardly in a systematic form; moreover, data for multi-component fuels at high pressure are even scarcer: filling this gap is the scope of the *Device for Hydrogen-Air Reaction Mode Analysis* (DHARMA) project, aiming at generating a comprehensive and coherent grid of data on the combustion properties of CH_4 and H_2, obtained in conditions as close as possible to those of actual engines.

The project relies on an optically accessible constant-volume bomb (static $P \leq 20$ MPa), where test are carried out on spherical expanding flames; the operating conditions (P_0, T_0), the equivalence ratio, the relative composition of the mixture, the ignition energy can be varied in a meaningful range. A shadowgraph setup, based on a c.w. laser source and a CMOS camera, is used to follow the flame growth with high time and space resolution.

The present work was carried out in the above-described framework and deals specifically with the effect of the initial pressure and of the H_2 amount on the combustion properties of CH_4-H_2-air mixtures.

The initial pressure varied between 3 and 18 bar; the H_2 percentage varied from 0% to 30% (vol.): the equivalence ratio ϕ was 1.0. These conditions were selected to match the operating range of automotive internal combustion engines.

The experimental tests yielded the (unstretched) laminar burning velocity and the Markstein length in each condition. These flame characteristics constitute a necessary input for the development and validation of theoretical models of laminar flame propagation. In addition, the interaction between laminar burning velocity and stretch (expressed by the Markstein length) allows to highlight the relation between flame and turbulence within the wrinkled thin laminar flamelet regime of premixed turbulent flames. These theoretical models, in turn, represent the basis for the design and testing of i.c. engines and/or combustors.

Other than the laminar burning characteristics, the phenomenon of flame instability has been explicitly analyzed, offering further details on flame properties. Under certain conditions, instability may wrinkle and break the flame front into small combustion cells: the effective flame front area increases, and the combustion process accelerates. Flame cellularity can be considered as an intermediate regime between laminar and turbulent combustion. Since its relevance in real combustion systems cannot be overlooked, the dependence of cellularity on both pressure and H_2 amount was suitably investigated.

2. Experimental Setup and Procedures

The general arrangement of the experimental layout is shown in Figure 1: a detailed description is given in [13]. The heart of the DHARMA laboratory is a constant-volume test reactor, made of stainless steel (AISI 316): the cylindrical chamber (i.d. = 70 mm, h = 90 mm, aspect ratio = 1.29) is rated for a maximum pressure of ≤ 20 MPa (static).

A total of 6 optical accesses are available: the larger viewports (d = 65 mm) are located normal to the chamber axis, providing nearly full access to chamber bore; smaller diameter ports are positioned on the chamber side, along two orthogonal axes. Hi-grade quartz windows (85 mm diameter, 30 mm thick) are installed in the main ports, the smaller side ports can be fitted either with quartz windows (49 mm diameter, 20 mm thick) or with a variety of stainless steel adapters (*i.e.*, transducers, electrodes, sampling ports, *etc.*).

Four additional service ports are available, e.g., for the intake of the combusting mixture and the vent of the exhaust gases.

The mixture is ignited with an automotive inductive ignition system (energy ≤ 60 mJ), which was characterized recording the time evolution of the voltage drop and the current flow between the electrodes: this allowed to evaluate the power and energy release. Being known the electrical

behaviour of the coil, the energy of discharge can be set in the range 0÷60 mJ, adjusting the time of charge (dwell time). The spark discharge takes place in the center of the chamber between two pointed-tip tungsten electrodes (dia. = 1 mm, gap = 1 mm).

Figure 1. Layout of the experimental apparatus.
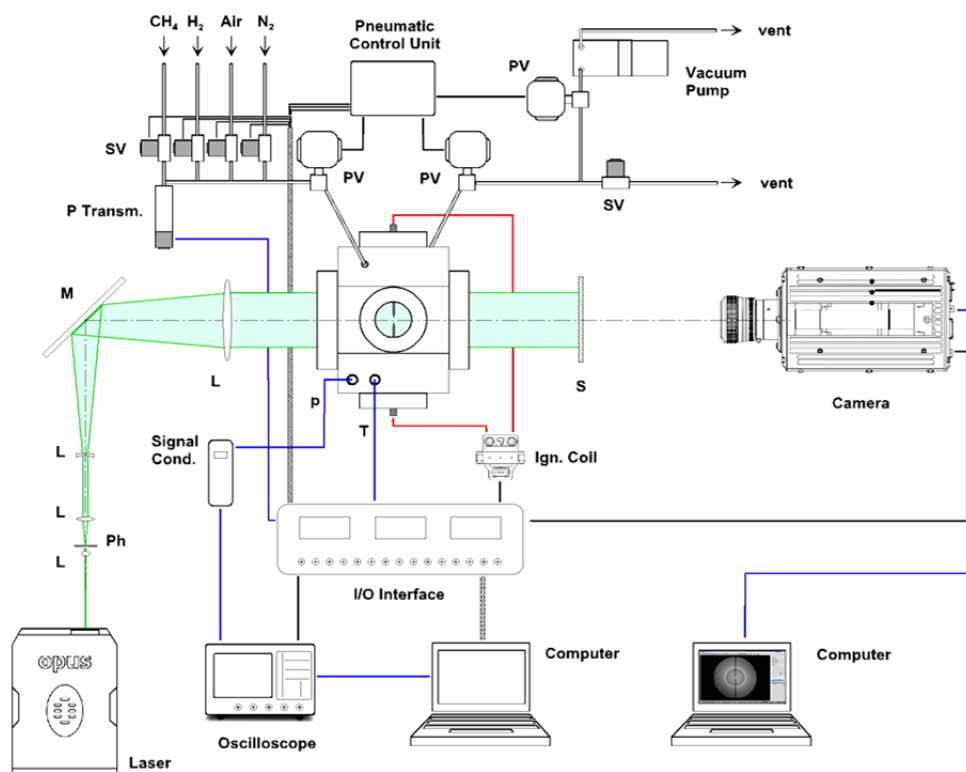
A high-frequency dynamic pressure transducer detects pressure history during the combustion events. A metal-shielded, type K thermocouple is used to monitor the temperature of the gases, save for the combustion phase.

The gas handling system was designed to prepare combustible mixtures of variable composition with high accuracy, spanning a range of initial pressures, which included values of relevance in spark-ignition engine operation.

High purity gases (CH$_4$: 99.9995%, H$_2$: 99.999%, dry air: 99.999%, N$_2$: 99.9995%) are used to prepare the mixtures, relying on the partial pressures method [2]: the amount of each gas is metered by a solenoid valve, controlled by a high-resolution (100 MHz) counter/timer board installed in the main computer. The pressure is monitored by a high-accuracy pressure transmitter (0–30 bar, accuracy ±0.08% FS). The gas supply system allows one to prepare combustible mixtures up to 30 bar. After each test, the system is vented, purged with N$_2$ and pumped down to 10^{-2} mbar. All the devices operate with a high degree of automation, to maximize safety and repeatability of the tests.

The entire lab conforms to current safety standards on the use of combustible gases, and is provided with interconnected gas leak sensors, cylinder cut-off devices and forced venting systems.

A parallel-beam direct shadowgraph layout [14] was set up for the analysis of spherical expanding flames. A Diode-Pumped Solid-State c.w. laser (2W @532nm) is used as the light source. High-resolution, time-resolved image acquisition is accomplished by means of a CMOS camera

(*Photron SA-5*, 1024 × 1024 pixel, 1,000,000 fps, shutter time ≥368 ns), interfaced to an independent workstation.

3. Evaluation of Laminar Parameters

3.1. Theory

Time-resolved, shadowgraph images of the spherical expanding flame allow to evaluate the laminar burning parameters, according to a well-known approach [2,5,7–10,12,15,16]. The time evolution of r_u (the flame radius on the *unburned* gas side) is obtained through frame-by-frame processing, assuming the luminous front in the shadowgraph corresponds to the radius on the unburned gas side [16].

The stretched flame speed V_s can then be evaluated as:

$$V_s = \frac{dr_u}{dt} \tag{1}$$

The obtained speed includes the stretch effects associated to the propagation of a flame surface, which experiences curvature and flow dynamic strain [17–22]. The flame stretch α is defined as the relative rate of change of the flame area: for a spherically expanding laminar flame it can be expressed as:

$$\alpha = \frac{1}{A}\frac{dA}{dt} = \frac{2}{r_u}\frac{dr_u}{dt} = 2\frac{V_s}{r_u} \tag{2}$$

The relationship between flame speed and stretch has been thoroughly investigated. It depends on the mathematical model and the associated hypotheses. A detailed analysis leads to the *nonlinear* formulation [23,24]:

$$\left(\frac{V_s}{V_{s0}}\right)^2 \ln\left(\frac{V_s}{V_{s0}}\right)^2 = -\frac{2L_b\alpha}{V_{s0}} \tag{3}$$

where V_{s0} is the unstretched flame speed and L_b is the burned gas Markstein length.

For weakly stretched flames, Equation (3) reduces to the *linear* formulation of [17,21]:

$$V_s = V_{s0} - L_b \cdot \alpha \tag{4}$$

By plotting V_s against α, it is possible to estimate (i) the unstretched flame speed V_{s0} as the value assumed by V_s at α = 0, and (ii) the Markstein length L_b as the gradient of the best straight line fit. The Markstein length indicates how and to what extent the flame is influenced by the stretch. Positive L_b are associated to flames with speed decreasing with stretch (which are stable), while in the case of negative L_b the flame speed tends to increase with stretch, becoming unstable; moreover, the magnitude of L_b indicates to what extent the flame propagation is influenced by the stretch.

The unstretched flame speed V_{s0} refers to the limiting case of a plane flame front, with infinite radius and negligible curvature: in such a case, V_{s0} can be related to the unstretched laminar burning velocity u_{l0} through the following relation:

$$u_{l0} = V_{s0}\frac{\rho_b}{\rho_u} \tag{5}$$

where ρ_b is the density of burned gases and ρ_u the density of unburned gases. Equation (5) holds true in the hypotheses of perfect gases, isobaric, adiabatic and equilibrium conditions.

The laminar flame thickness δ_l is a characteristic length, rather than an actual physical dimension: it's meant to describe the extension of a reaction zone and different definitions have been proposed, based on the balance of mass, energy or momentum. In the current work, the hydrodynamic thickness has been used:

$$\delta_l = \frac{v_u}{u_{l0}} = \frac{\mu_u}{\rho_u \cdot u_{l0}}$$

(6)

where v_u and μ_u are respectively the kinematic and dynamic viscosity of the unburned mixture [6].

3.2. Data Analysis and Processing

An image processing routine has been implemented to infer the flame radius r_u from the shadowgraph data: for each frame, the flame contour is traced and the area of the projected flame ball is evaluated; the radius is estimated as that of a circle of equal area to the flame. The time evolution of the flame radius r_u offers the basis for the evaluation of the laminar parameters (u_{l0} and L_b).

In the present work, a linear dependence was assumed between the flame speed and the stretch, Equation (4): the validity of this postulation was corroborated "a posteriori" by the results.

The usual approach for the linear analysis consists of a series of steps, which makes use of Equations (1),(2),(4) and (5): a polynomial fit of r_u data is first performed; differentiation of the fit allows to obtain the stretched flame speed V_s defined in Equation (1); being known V_s and r_u, the stretch rate α can be evaluated after Equation (2); according to Equation (4), linear-fit extrapolation of the flame speed to $\alpha = 0$ gives the unstretched flame speed V_{s0}, while the slope of the fit allows to estimate the burned gas Markstein length L_b. The critical step in this approach resides in the polynomial differentiation, which is highly sensitive to the choice of the original data interval: this may introduce noise and lead to distorted profiles of V_s, affecting both V_{s0} and L_b.

At least two different approaches have been proposed in the literature [25,26] for an analytical solution, allowing to obtain both the unstretched flame speed and the Markstein length, directly from the time evolution of the flame radius. Following the method of Tahtouh *et al.* [26], Equations (1) and (4) can be rearranged as:

$$\frac{dr}{dt} = V_{s0} - 2L_b \frac{dr}{rdt}$$

(7)

The solution to Equation (7) is:

$$r(t) = 2L_b W(Z)$$

(8)

where W is the Lambert function, and Z is given by:

$$Z = \frac{e^{\frac{V_{s0} \cdot t + C_1}{2L_b}}}{2L_b}$$

(9)

C_1 is a constant to be determined.

The values of V_{s0} and L_b (along with C_1) are obtained minimizing the following equation:

$$\sum_{1}^{N}\left(r_u(t)-r(t)\right)^2 = \sum_{1}^{N}\left(r_u(t)-2L_bW(Z)\right)^2 \tag{10}$$

where r_u is the experimentally measured radius. The Lambert function W is a multi-valued function [27]: if Z is real, for $-1/e \leq Z < 0$ $W(Z)$ can assume two possible real values. The branch satisfying the condition $-1 \leq W(Z)$ is termed the *principal* branch and denoted $W_0(Z)$. The branch satisfying the condition $W(Z) \leq -1$ is called the *alternate* branch and denoted $W_{-1}(Z)$. For $L_b > 0$ (that is $Z > 0$), the principal branch of the Lambert function (W_0) must be used, while for $L_b < 0$, $W_{-1}(Z)$ should be used. This method delivers directly V_{s0} and L_b for each test case. The stretched flame speed and the stretch rate can be obtained differentiating Equation (8) with respect to time.

4. Laminar Burning Properties

The following results refer to the combustion behaviour of CH_4 and of CH_4-H_2 mixtures, with a H_2 fraction of 20% and 30% in volume: these values optimize the trade-off between additional technical complexity and performance benefits, allowing for a direct utilization of CH_4-H_2 mixtures in current natural gas engines [28,29]. The initial temperature T_0 varied in the range 293÷305 K, while the initial pressure P_0 was set at 3, 6, 12 and 18 bar (abs.). The study was limited to stoichiometric air-fuel mixtures (equivalence ratio $\phi = 1.0$), since it was targeted to the development of automotive internal combustion engines, operating with closed-loop three-way catalyst.

Time-resolved shadowgraph images of spherical expanding flames were used to infer the laminar flame parameters. As stated earlier, laminar analysis can be meaningfully carried out in the constant-pressure phase only, before the chamber pressure shows a sensible increment. Moreover, as stated by Bradley *et al.* [6], the early stages of the flame kernel growth are affected by the spark energy release, and cannot be taken into account in the evaluation of laminar flame properties.

The resulting measurement time-window starts after the ignition disturbances are over, and ends when the pressure shows an appreciable rise. In the present tests, spark energy was set at 20 mJ (electrical). Since the ignition system is inductive, only a small fraction of this energy is released in the breakdown phase (<10 ns), which (due to the high power peaks) drives the early kernel growth and induces likely perturbations in the flame [30,31]. Given the small spark energy, the extent of the ignition disturbances can be expected to be accordingly limited.

Analysis of the flame radii in the early stages revealed no discernible evidence of ignition-induced effects: nonetheless, pending further investigation, a conservative criterion was applied, based on the morphology of the flame: flames with an aspect ratio (major axis/minor axis of the fitting ellipse) lower than 0.98 were discarded. Typical value for the minimum radius was about 4.5 mm.

As stated above, the maximum radius was obtained applying the constraint of constant pressure: typical value was ~9.5 mm, corresponding to ~27% of the chamber radius. This value meets the ($r_u < 0.3r_{chamber}$) criterion suggested by Burke *et al.* [32] to avoid the effects of confinement in a cylindrical chamber.

Figure 2 shows three sets of frames, each set coming from a single combustion event: they illustrate the flame development in the constant-pressure phase, at $P_0 = 3$ bar. The combustion behaviour is

compared for CH_4 and H_2-CH_4 mixtures with a H_2 content of 20% and 30% (vol.). Recording speed was 7000 fps (143 μs between consecutive frames) with a shutter speed of 1 μs; optical magnification ratio was 3.27:1, resulting in a spatial resolution of 15.3 pixel/mm. Flames appear smooth and virtually free of wrinkles; the crack shown for the 30% mixture is the self-similar development of initial ignition disturbances. The effect of H_2 addition can be appreciated in the increased size of the flame ball at a given time.

Figure 2. Flame propagation in the isobaric phase for stoichiometric CH_4 and H_2-enriched mixtures (20% and 30% vol.) at 3 bar and room temperature. Window dia. 65 mm.
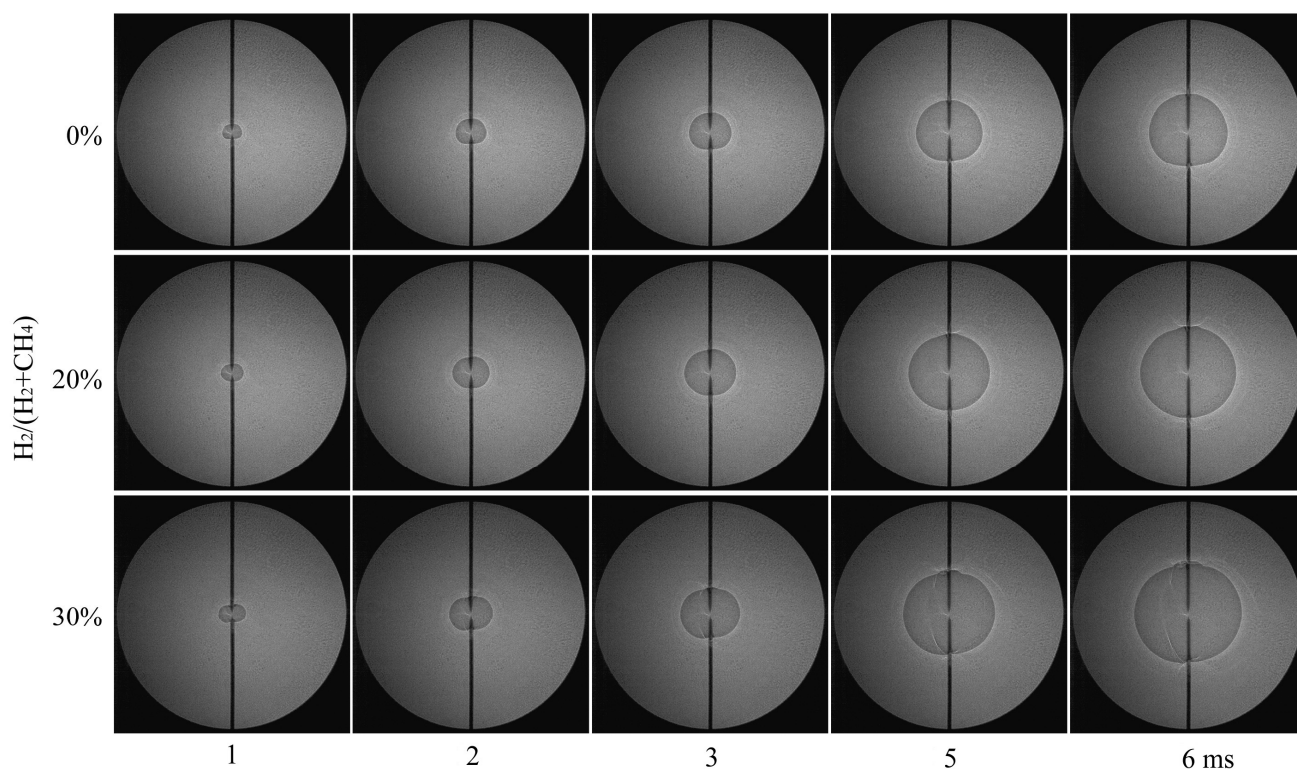
The output of shadowgraph image processing is shown in Figure 3: the time-evolution of the flame radius is compared for CH_4 and CH_4-H_2 mixtures, at different starting pressure: each set of data corresponds to a single, time-resolved combustion event, which has been selected as representative of the test point (P_0, T_0, % H_2, ϕ). The useful range for data analysis is highlighted in colour for each case: grayed-out data were discarded in the extraction of laminar parameters.

As mentioned earlier, the analytical solution delivers V_{s0} and L_b directly. The time evolution of V_s can anyway be evaluated differentiating Equation (8). This allows one to trace the behavior of the stretched flame speed against α, as shown in Figure 4 for the same test cases and conditions of Figure 3. Figure 4 clearly shows the effect of the starting pressure and of the Hydrogen amount on the flame behaviour: increasing the pressure has a detrimental effect on the flame speed; on the contrary, the addition of H_2, even in limited amounts, has always a positive effect on the flame speed.

Figure 3. Time evolution of flame radius. Stoichiometric CH_4 and H_2-enriched mixtures (20% and 30% vol.) at room temperature. Starting pressure as indicated.
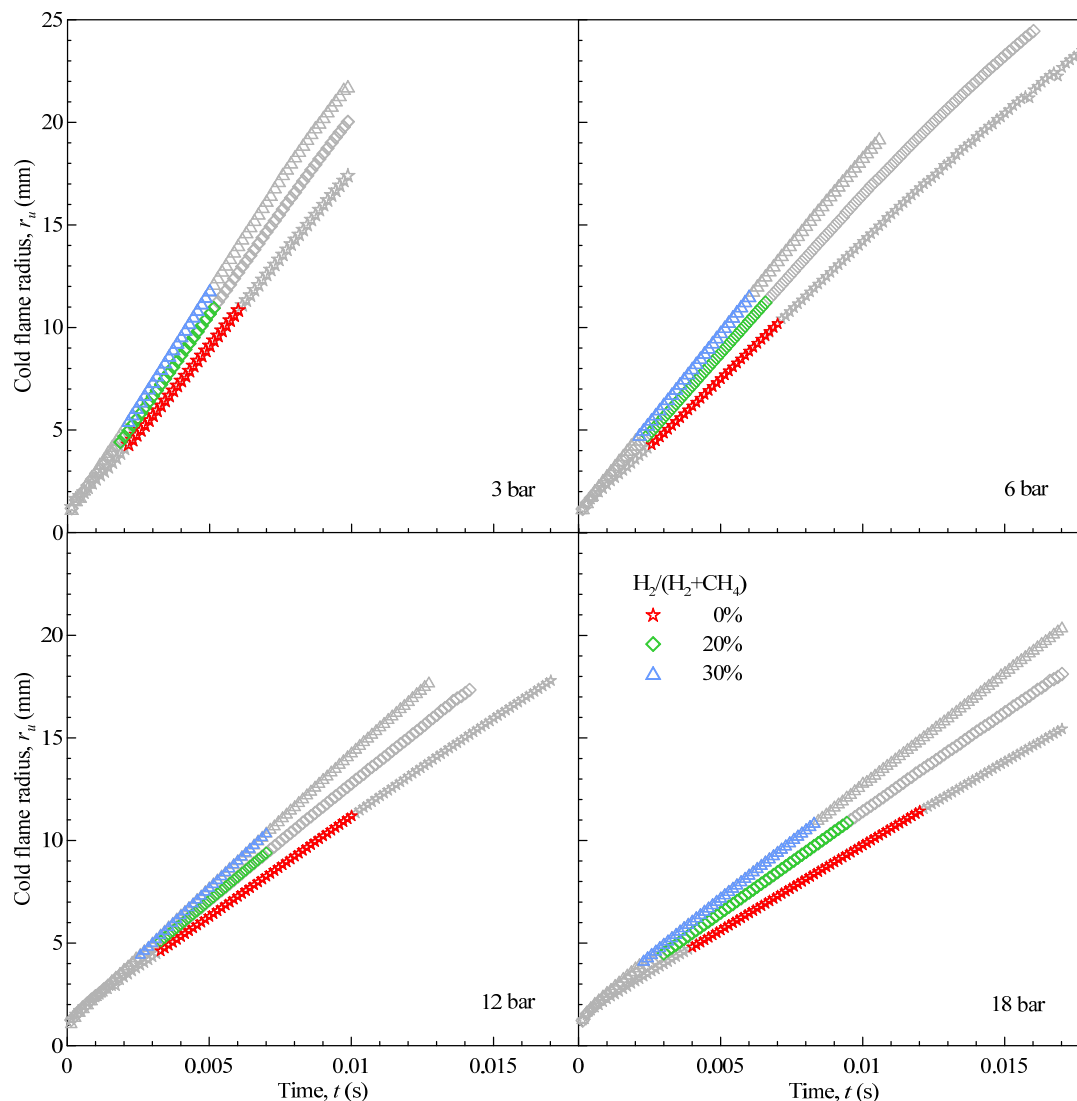
The unstretched laminar burning velocity u_{l0} was calculated with Equation (5). In a recent paper [33], Varea *et al*. proposed a new approach for the measurement of u_{l0}, which bypass the evaluation of the expansion factor. The authors highlighted the drawbacks of the approach generally used in the literature, which requires the evaluation of the ratio ρ_u/ρ_b: this can introduce errors if any of the hypotheses behind Equation (5) are not satisfied. In the case of CH_4, they concluded that the "old" method delivers reliable results. In the present work, the expansion factor was obtained from the properties of the reactant species and of equilibrated adiabatic products, evaluated with the GASEQ code [34].

Figure 4. Evolution of the flame speed *versus* flame stretch. Same cases as Figure 3.
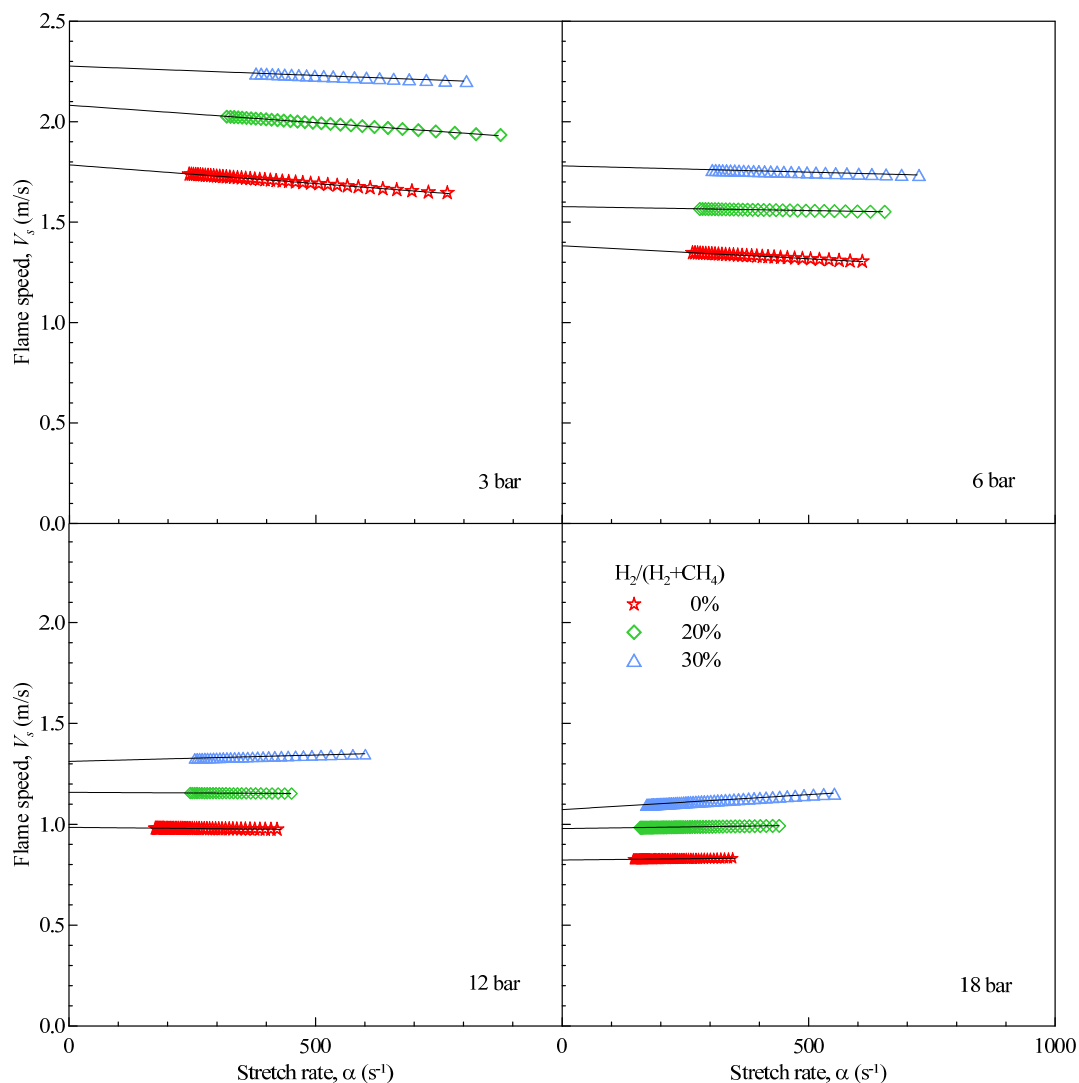
The u_{l0} values for CH_4 are summarized in Figure 5 as a function of initial pressure P_0. As the starting pressure is increased from 3 to 18 bars, a decrease of the laminar burning velocity can be observed; u_{l0} at 18 bar is about 40% of 3 bar. The comparison is proposed with the results from other research groups [3,4,7–11]. Data at high pressures are less readily available than atmospheric pressure: the present results for u_{l0} show a fairly good agreement with most of published data, save for the values of Halter, which appear slightly lower.

The variation of the burning velocity with initial pressure and temperature can be expressed by the simple empirical correlation [8,10]:

$$u_{l0} = u_{l0,r}\left(\frac{P_0}{P_{0,r}}\right)^{\beta}\left(\frac{T_0}{T_{0,r}}\right)^{\gamma} \tag{11}$$

where $u_{l0,r}$ is the laminar burning velocity at the reference temperature $T_{0,r}$ and pressure $P_{0,r}$. In the present study, only the pressure dependence was evidenced.

The parameter β was optimized in the range 3÷18 bar, using 3 bar as the reference pressure. As shown in Figure 6, the results are well described by Equation (11): the coefficient of determination R^2

is >0.99. In the case of CH_4 the value of β is −0.45, which is bracketed between the findings of Gu *et al.* [8] and Halter *et al.* [10]. CH_4-H_2 mixtures show a minor reduction in the magnitude of β, which is proportional to the amount of H_2.

Figure 5. Unstretched laminar burning velocity as a function of the starting pressure, for stoichiometric CH_4 at room temperature.
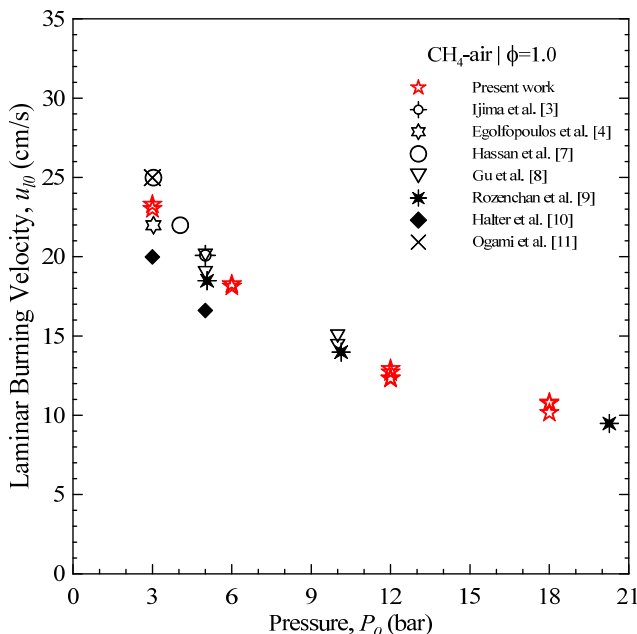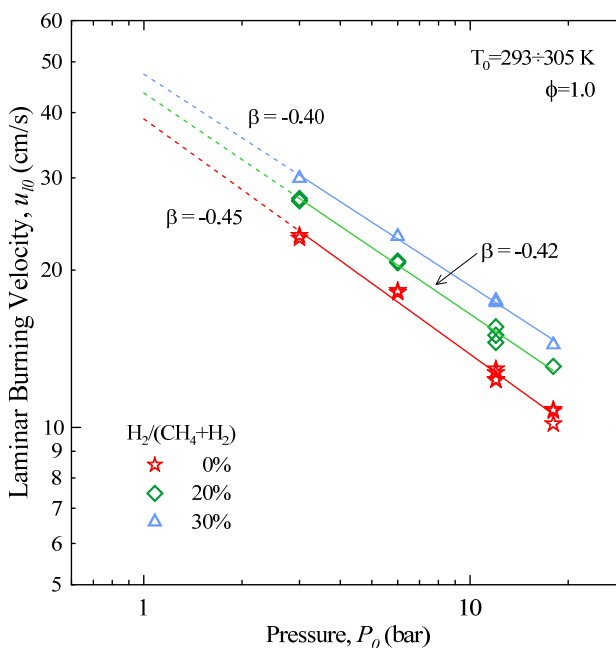

Figure 6. Effect of initial pressure on the unstretched laminar burning velocity. Solid lines represent fits obtained by Equation (11): values of β as indicated.

The effect of the addition of H_2 to CH_4 is twofold: the laminar burning velocity not only increases but becomes also less sensitive to the initial pressure.

The Markstein length is shown in Figure 7 as a function of the starting pressure. In the case of CH_4 at lower pressure, L_b is positive, corresponding to a flame speed which increases as α decreases. As the pressure is increased, the Markstein length becomes smaller, and eventually negative: this result is in agreement with the findings of Gu *et al.* [8], who reported on CH_4 flames up to 10 bar. The effect is probably related to the decrease of flame thickness associated to the pressure increment: this reduces the effect of curvature in counteracting the hydrodynamic instabilities.

Figure 7. Burned-gas Markstein length as a function of the starting pressure, for stoichiometric CH_4 and H_2-enriched mixtures at room temperature.
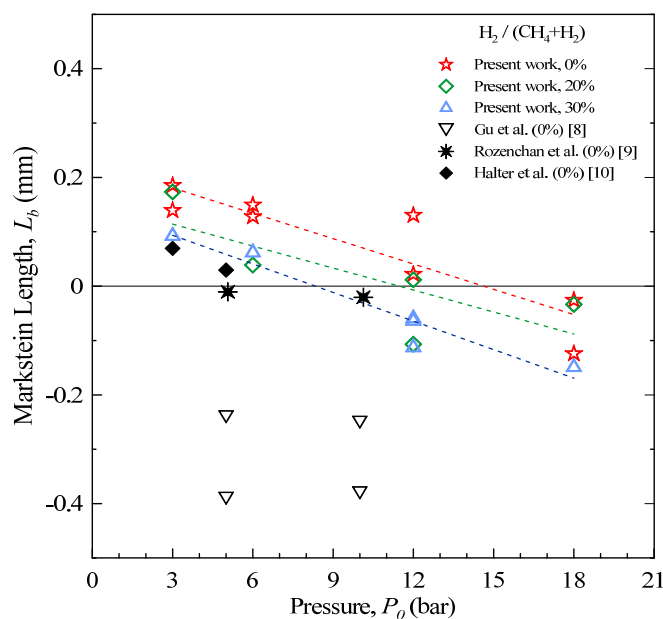
The addition of H_2 to CH_4 has the anticipated effect [6] of lowering the Markstein length, since the mixture thermal equidiffusivity is altered.

Due to the combined effects of initial pressure and Hydrogen content, high-pressure CH_4-H_2 flames are characterized by the lowest values of L_b.

The obtained results confirm the selected procedure for data analysis as appropriate. Since $-0.2 \leq L_b \leq 0.2$ mm, and the minimum flame radius used in the image processing is ~4.5 mm, the ratio $|L_b/r_{u\,min}|$ results lower than ~0.045. According to Halter *et al.* [24], this legitimate the use of the *linear* approach, as the relative error respect to the *nonlinear* approach is negligible.

5. Flame Stability and Cellular Structures

The burned-gas Markstein length L_b expresses how and how much the stretch rate affects the flame propagation. Aerodynamic stretch, induced by flame curvature, interacts with the propensity of the flame to develop instability (hydrodynamic and/or thermo diffusive). In this sense, L_b can be considered an indicator of flame instability. Interestingly enough, the Markstein length is evaluated from the expanding flame in the constant-pressure regime, when the flame is smooth and there is little or no distortion (see e.g., Figure 2). In other words, L_b has a predictive nature.

Evidence of flame instability, if any, appears afterwards, depending on the experimental setup. The flame travelling the chamber volume may go through various morphological alterations, characterized by the appearance and branching of large cracks and, eventually, fine cellular structures [35–41]. Figure 8 shows three sets of frames at selected times after the spark: they were obtained in the case of pure and H_2-enriched CH_4 mixtures, ignited at $P_0 = 6$ bar. Recording conditions were as in Figure 2.

Figure 8. Evolution of flame instability for stoichiometric CH_4 and H_2-enriched mixtures (20% and 30% vol.). $P_0 = 6$ bar, $T_0 = 298$ K. Window dia. 65 mm.
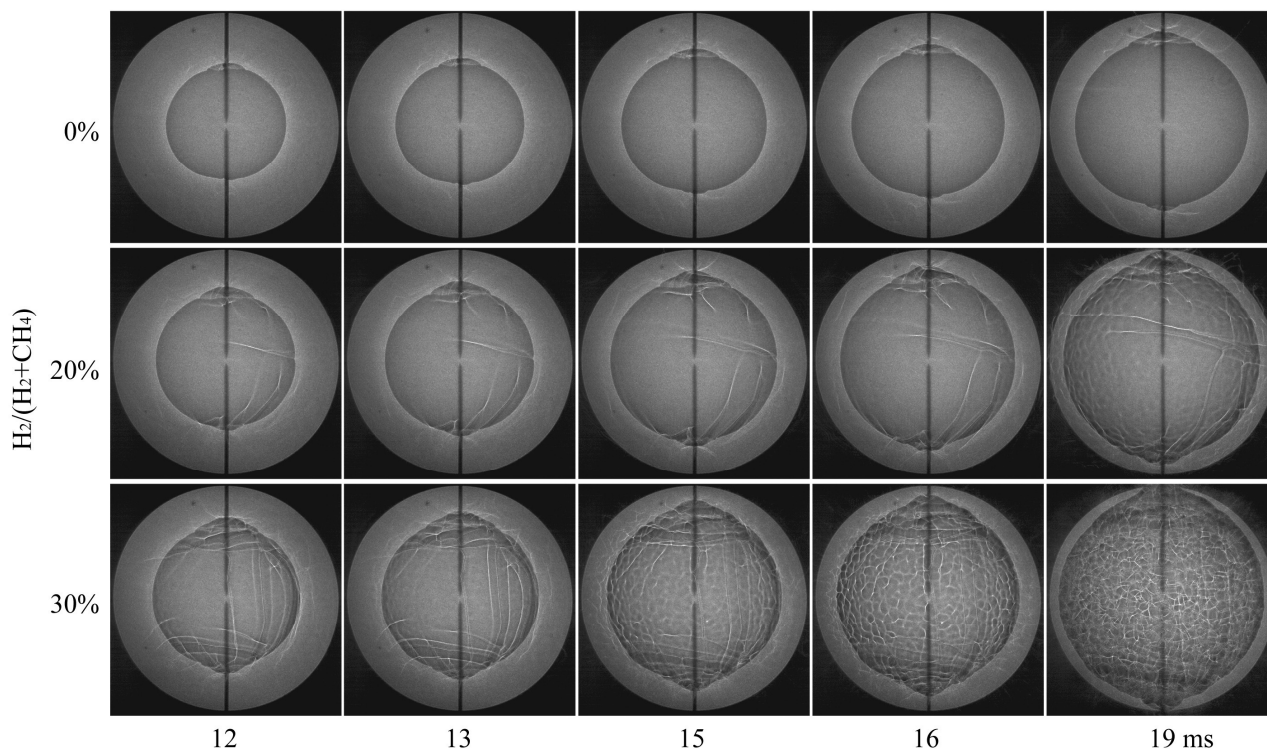

It is worth stressing that these images refer to late stages of flame propagation, when the combustion process is no more isobaric.

At moderate values of the initial pressure ($P_0 = 6$ bar), the CH_4 flame keeps its laminar shape until it approaches the chamber walls. The addition of H_2 to the mixture, even in limited amount (20%), corresponds to the appearance of large cracks on the flame surface. This effect gets more striking as long as the flame travels the chamber, with the cracks being suddenly integrated by cellular structures [36,40].

As shown in Figure 7, when the initial pressure is increased, the Markstein length decreases, suggesting that flame instability should increase. This is confirmed by Figure 9, which reports three sets of frames obtained for mixtures ignited at $P_0 = 12$ bar: no matter the mixture composition, in all the cases the flame exhibits deviations from a smooth, laminar morphology. These phenomena take place earlier in the process (that is at smaller radii), if compared to $P_0 = 6$ bar. The typical sequence of large cracks followed by smaller, uniformly distributed "cells" is always present; if the amount of H_2 is increased, cellular structures show up at earlier times.

Figure 9. Evolution of flame instability for stoichiometric CH_4 and H_2-enriched mixtures (20% and 30% vol.). $P_0 = 12$ bar, $T_0 = 298$ K. Window dia. 65 mm.
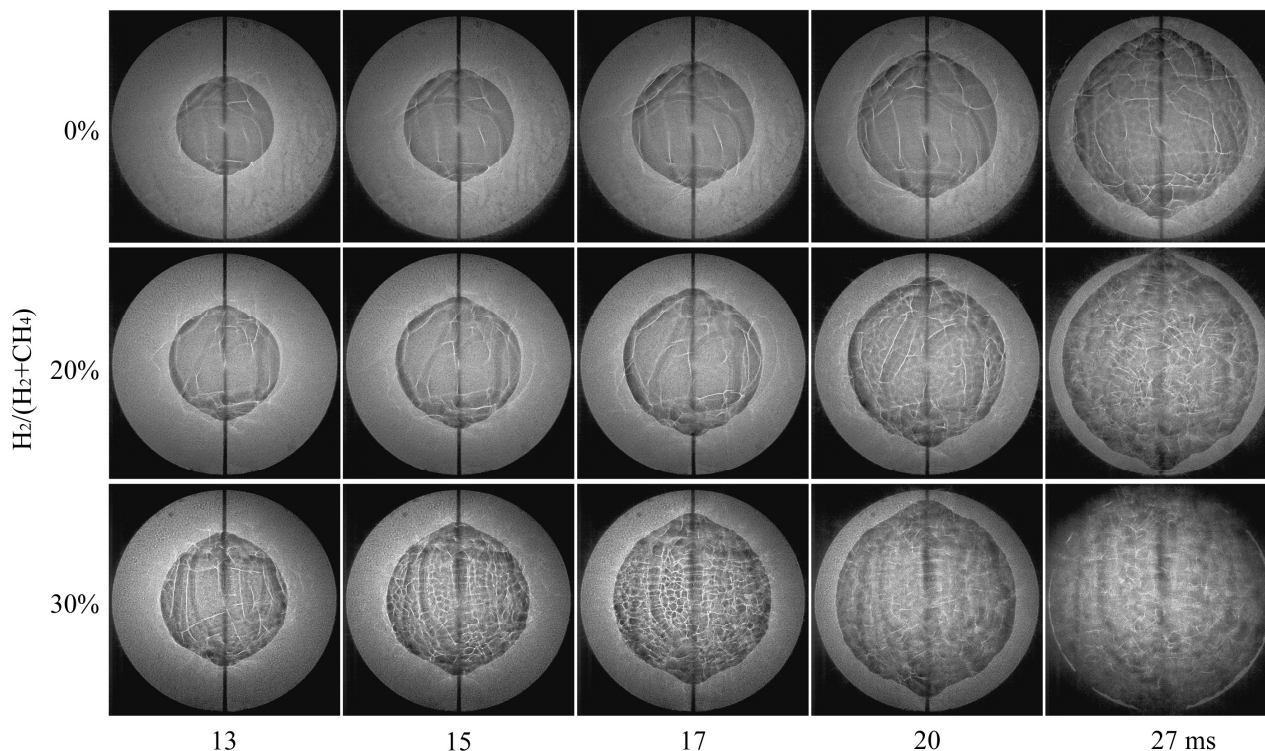
As suggested by Law *et al.* [39], two characteristic instants can be identified: the first is related to the branching of large cracks across the flame surface, the second to the sudden appearance of cells, almost uniformly over the same surface, with a characteristic size much smaller than the large cracks. Following the convention of Law *et al.* [39], we chose to adopt the second instant as representative of the flame loosing stability: this allows to define the critical radius r_{cr} for the onset of instability.

Figure 10 reports the values of r_{cr} as a function of the starting pressure, for different mixture compositions. All the flames at $P_0 = 3$ bar show a laminar behaviour, hence the lack of data points for this case.

At $P_0 = 6$ bar, CH_4 flames show the appearance of cellular structures when the flame approaches the chamber wall: these points are greyed-out, since they are likely influenced by additional phenomena, like flame-wall interaction.

These results show that increasing the pressure, the critical radius gets smaller: the resulting picture is of a flame that departs earlier from the laminar regime, and mostly develops under a wrinkled regime. Adding H_2 to CH_4 further reduces r_{cr} (*i.e.*, increases instability), even if the effect gets less marked as the pressure is increased: adding 30% of H_2 to CH_4 reduces r_{cr} by 24% at 12 bar and by 21.5% at 18 bar.

The morphological analysis appears to confirm the trends from the flame stretch analysis. As shown in Figure 11, the critical radius r_{cr} exhibits a reasonable correlation with the Markstein length L_b.

As far as the observed instabilities are concerned, it is well established that flame cellularity can be hydrodynamic and thermo-diffusional in nature (if body-force effects are absent).

Figure 10. Critical radius for the onset of flame instability as a function of the starting pressure, for stoichiometric CH_4 and H_2-enriched mixtures at room temperature.
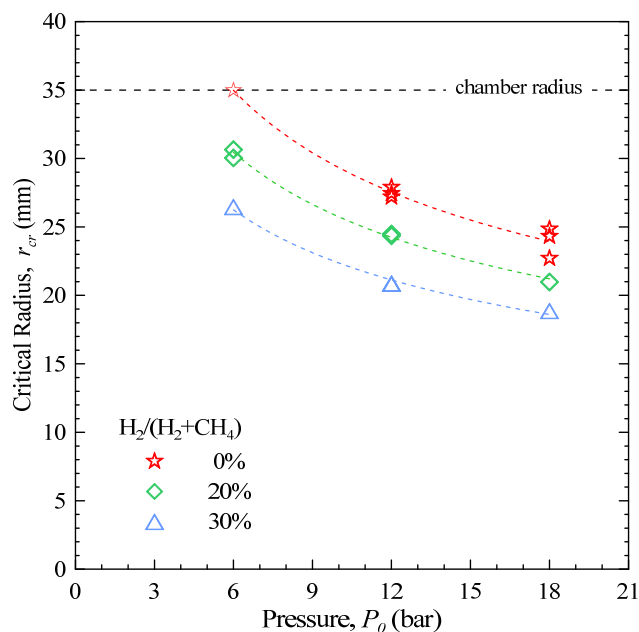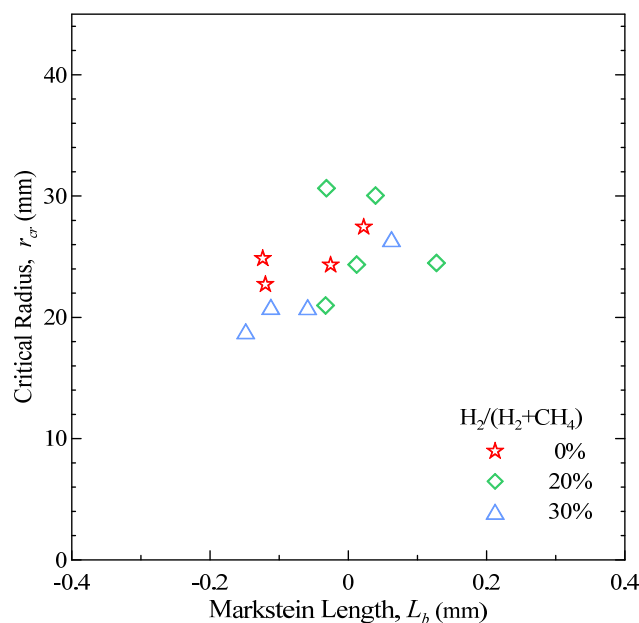

Figure 11. Critical radius for the onset of flame instability *versus* Markstein length.

Hydrodynamic instability is caused by the density difference across the flame. It is expressed by the thermal expansion ratio of the burned to the unburned mixtures, and is always present for all flames [38].

Thermo-diffusional instability originates from the diffusive disparity of heat conduction from the flame and reactant diffusion towards the flame; it may not be present, if the flame is equidiffusive [21]. The mixture parameter representing the effect of non-equidiffusion is the global Lewis number, *Le*, defined as the ratio of the heat diffusivity of the mixture to the mass diffusivity of the limiting reactant

to the abundant inert [20–22]. Values of *Le* > 1, =1 and <1 correspond to flames which are diffusionally stable, neutral of unstable, respectively.

In the case of a spherical expanding flame, cellular instability is initially suppressed by the strong curvature-induced stretch, associated with the corresponding small flame radii. As the flame expands, the stretch decreases, until a condition is reached in which cell development can no longer be suppressed and cells suddenly appear over the flame surface. This state depends on the combined effects of the hydrodynamic and diffusional–thermal instabilities.

The above-described transition can be expressed in terms of the critical Peclet number, obtained scaling the critical radius r_{cr} by the laminar flame thickness δ_l. An expression has been proposed of Pe_{cr} as the sum of two terms, corresponding to hydrodynamic and diffusional–thermal instabilities [40].

Being known r_{cr} and L_b, the comparison can be drawn between the Markstein number (defined as L_b/δ_l) and Pe_{cr}: the results are shown in Figure 12.

Actually, in the present conditions, expressing the comparison in terms of non-dimensional parameters does not add to a better understanding of the phenomena.

Figure 12. Critical Peclet number *versus* Markstein number.
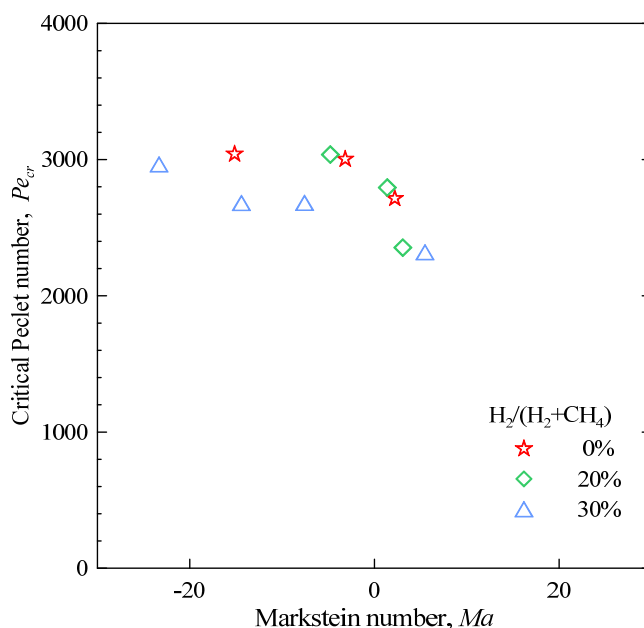
As shown in Figure 12, the almost constant value of Pe_{cr} suggests the flames are equidiffusive in nature [40], yet negative values of *Ma* stand for *Le* < 1: such values correspond to flames where the deficient reactant is the more diffusive one, so that thermo-diffusive instability (of cellular nature) is promoted. Then one should expect Pe_{cr} to increase with *Le*, but data show a reversed trend.

The described behaviour prevents a straightforward identification of the role of the hydrodynamic and thermo-diffusive terms in the global Pe_{cr}. Pending a deeper theoretical analysis, a possible explanation of this apparent incongruity could reside in the different conditions in which L_b and r_{cr} have been evaluated: while the former is a parameter obtained in the isobaric phase of flame development, the latter was measured later, when the global pressure in the chamber was increasing.

The unpredictability of the results could be due to the scaling by δ_l, since this parameter is meaningfully defined in the isobaric phase.

6. Conclusions

The effect of the initial pressure and of the H_2 content on the combustion of CH_4-H_2-air mixtures was investigated studying spherical expanding flames. Laminar burning parameters (unstretched burning velocity, burned-gas Markstein length) and flame instability characteristics (critical radius for the onset of cellularity) were evaluated for mixtures with different H_2 percentage (0%, 20% and 30% vol.), equivalence ratio $\phi = 1.0$, initial temperature $T_0 = 293 \div 305$ K and initial pressure $P_0 = 3 \div 18$ bar.

The obtained results allowed to assess quantitatively the effect of pressure and of H_2 amount: the laminar burning velocity was found to decrease with the former and increase with the latter. The flame stability decreased when any of the two parameters was increased.

The laminar burning velocity and the Markstein length were found to be in good agreement with published data, wherever available. As a matter of fact, the present results extend the data published so far in literature, as far as high-pressure, stoichiometric H_2-enriched mixtures are concerned.

In agreement with the observed behaviour of the Markstein length, the results on flame cellularity highlight the increasing relevance of the phenomenon at high pressures and/or for significant concentrations of hydrogen.

The main findings can be summarized as follows:

- If the initial pressure is increased, the laminar burning velocity decreases and the Markstein length becomes negative. In the case of CH_4, when P_0 is raised from 3 to 18 bar, u_{l0} decreases by ~40%. In the same conditions, L_b shifts from about 0.20 to −0.07.
- If H_2 is added to CH_4, the burning velocity increases. At $P_0 = 3$ bar, u_{l0} increases by ~25% if the amount of H_2 in the mixture is 30%. The Markstein length of H_2-enhanced mixtures is shifted to smaller values, if compared to pure CH_4, and becomes negative at $P_0 > 6$ bar.
- The behaviour of u_{l0} *vs.* P_0 follows a power law, with exponent $\beta = -0.45$ for CH_4. The magnitude of β decreases with the amount of H_2.
- The critical radius for the onset of cellularity was found to decrease when either the pressure or the H_2 content in the mixture were increased. At $P_0 = 3$ bar, regardless of the amount of H_2, no sign of instability was observed; at $P_0 > 6$ bar, the flame get increasingly unstable with the amount of H_2. The critical radius shows a good correlation with the Markstein length.

The present findings offer a quantitative frame of reference for the burning properties of CH_4-H_2, highlighting the specific features of the combustion process in condition typical of i.c. engines.

Acknowledgments

References

1. Lewis, B.; von Elbe, G. Determination of the speed of flames and the temperature distribution in a spherical bomb from time-pressure explosion records. *J. Chem. Phys.* **1934**, *2*, 283–290.
2. Milton, B.E.; Keck, J.C. Laminar burning velocities in stoichiometric hydrogen and hydrogen-hydrocarbon gas mixtures. *Combust. Flame* **1984**, *58*, 13–22.
3. Ijima, T.; Takeno, T. Effects of temperature and pressure on burning velocity. *Combust. Flame* **1986**, *65*, 35–43.
4. Egolfopoulos, F.N.; Cho, P.; Law, C.K. Laminar flame speeds of methane-air mixtures under reduced and elevated pressures. *Combust. Flame* **1989**, *76*, 375–391.
5. Dowdy, D.R.; Smith, D.B.; Taylor, S.C.; Williams, A. The use of expanding spherical flames to determine burning velocities and stretch effects in hydrogen/air mixtures. *Symp. (Int.) Combust.* **1991**, *23*, 325–332.
6. Bradley, D.; Gaskell, P.H.; Gu, X.J. Burning velocities, markstein lengths, and flame quenching for spherical methane-air flames: A computational study. *Combust. Flame* **1996**, *104*, 176–198.
7. Hassan, M.I.; Aung, K.T.; Faeth, G.M. Measured and predicted properties of laminar premixed methane/air flames at various pressures. *Combust. Flame* **1998**, *115*, 539–550.
8. Gu, X.J.; Haq, M.Z.; Lawes, M.; Woolley, R. Laminar burning velocity and markstein lengths of methane-air mixtures. *Combust. Flame* **2000**, *121*, 41–58.
9. Rozenchan, G.; Zhu, D.L.; Law, C.K.; Tse, S.D. Outward propagation, burning velocities, and chemical effects of methane flames up to 60 atm. *Proc. Combust. Inst.* **2002**, *29*, 1461–1469.
10. Halter, F.; Chauveau, C.; Djebaili-Chaumeix, N.; Gokalp, I. Characterization of the effects of pressure and hydrogen concentration on laminar burning velocities of methane-hydrogen-air mixtures. *Proc. Combust. Inst.* **2005**, *30*, 201–208.
11. Ogami, Y.; Kobayashi, H. Laminar burning velocity of stoichiometric CH_4/air premixed flames at high-pressure and high-temperature. *JSME Int. J. B* **2005**, *48*, 603–609.
12. Verhelst, S.; Woolley, R.; Lawes, M.; Sierens, R. Laminar and unstable burning velocities and Markstein lengths of hydrogen-air mixtures at engine-like conditions. *Proc. Combust. Inst.* **2005**, *30*, 209–216.
13. Moccia, V.; D'Alessio, J. *Evaluating the Burning Velocity of Gaseous Fuels for Engine Applications: the DHARMA Project*; SAE Technical Paper 2011-24-0056; 2011, doi:10.4271/2011-24-0056.
14. Settles, G.S. *Schlieren and Shadowgraph Techniques*; Springer: Berlin, Germany, 2001.
15. Huang, Z.; Zhang, Y.; Zeng, K.; Liu, B.; Wang, Q.; Jiang, D. Measurements of laminar burning velocities for natural gas-hydrogen-air mixtures. *Combust. Flame* **2006**, *146*, 302–311.
16. Parsinejad, F.; Keck, J.; Metghalchi, H. On the location of flame edge in Shadowgraph pictures of spherical flames: A theoretical and experimental study. *Exp. Fluids* **2007**, *43*, 887–894.
17. Markstein, G.H. Experimental and theoretical studies of flame-front stability. *J. Aernaut. Sci.* **1951**, *18*, 199–209.
18. Karlovitz, B.; Denniston, D.W., Jr.; Knapschaefer, D.H.; Wells, F.E. Studies on turbulent flames: A. Flame propagation across velocity gradients, B. Turbulence measurement in flames. *Symp. (Int.) Combust.* **1953**, *4*, 613–620.

19. Strehlow, R.A.; Savage, L.D. The concept of flame stretch. *Combust. Flame* **1978**, *31*, 209–211.

20. Matalon, M. On flame stretch. *Combust. Sci. Technol.* **1983**, *31*, 169–181.

21. Clavin, P. Dynamic behavior of premixed flame fronts in laminar and turbulent flows. *Prog. Energy Combust.* **1985**, *11*, 1–59.

22. Law, C.K.; Sung, C.J. Structure, aerodynamics, and geometry of premixed flamelets. *Prog. Energy Combust.* **2000**, *26*, 459–505.

23. Chen, Z.; Ju, Y. Theoretical analysis of the evolution from ignition kernel to flame ball and planar flame. *Combust. Theory Model* **2007**, *11*, 427–453.

24. Halter, F.; Tahtouh, T.; Mounaïm-Rousselle, C. Nonlinear effects of stretch on the flame front propagation. *Combust. Flame* **2010**, *157*, 1825–1832.

25. Burluka, A.A.; Fairweather, M.; Ormsby, M.B.; Sheppard, C.G.W; Wooley, R. The Laminar Burning Properties of Premixed Hydrogen-Air Flames Determined Using a Novel Analysis method. In *Proceedings of Third European Combustion Meeting (ECM 2007)*, Crete, Greece, 11–13 April 2007.

26. Tahtouh, T.; Halter, F.; Mounaïm-Rousselle, C. Measurement of laminar burning speeds and Markstein lengths using a novel methodology. *Combust. Flame* **2009**, *156*, 1735–1743.

27. Corless, R.M.; Gonnet, G.H.; Hare, D.E.G.; Jeffrey, D.J.; Knuth, D.E. On the Lambert W function. *Adv. Comput. Math.* **1996**, *5*, 329–359.

28. Akansu, S.O.; Kahraman, N.; Çeper, N. Experimental study on a spark ignition engine fuelled by methane-hydrogen mixtures. *Int. J. Hydrog. Energy* **2007**, *32*, 4279–4284.

29. Kahraman, N.; Çeper, B.; Akansu, S.O.; Aydin, K. Investigation of combustion characteristics and emissions in a spark-ignition engine fuelled with natural gas-hydrogen blends. *Int. J. Hydrog. Energy* **2009**, *34*, 1026–1034.

30. Maly, R.; Vogel, M. Initiation and propagation of flame fronts in lean CH_4-air mixtures by the three modes of the ignition spark. *Symp. (Int.) Combust.* **1979**, *17*, 821–831.

31. Borghese, A.; Diana, M.; Moccia, V.; Tamai, R. Early growth of flames, ignited by fast sparks. *Combust. Sci. Technol.* **1991**, *76*, 219–231.

32. Burke, M.P.; Chen, Z.; Ju, Y.; Dryer, F.L. Effect of cylindrical confinement on the determination of laminar flame speeds using outwardly propagating flames. *Combust. Flame* **2009**, *156*, 771–779.

33. Varea, E.; Modica, V.; Vandel, A.; Renou, B. Measurement of laminar burning velocity and Markstein length relative to fresh gases using a new postprocessing procedure: Application to laminar spherical flames for methane, ethanol and isooctane/air mixtures. *Combust. Flame* **2012**, *159*, 577–590.

34. GASEQ. *A Chemical Equilibrium Program for Windows*. Available online: http://www.c.morley. dsl.pipex.com/ (accessed on 5 July 2012).

35. Groff, E.G. The cellular nature of confined spherical propane-air flames. *Combust. Flame* **1982**, *48*, 51–62.

36. Bradley, D.; Harper, C.M. The development of instabilities in laminar explosion flames. *Combust. Flame* **1994**, *99*, 562–572.

37. Tse, S.D.; Zhu, D.L.; Law, C.K. Morphology and burning rates of expanding spherical flames in H_2/O_2/inert mixtures up to 60 atmospheres. *Proc. Combust. Inst.* **2000**, *28*, 1793–1800.

38. Kwon, O.C.; Rozenchan, G.; Law, C.K. Cellular instabilities and self-acceleration of outwardly propagating spherical flames. *Proc. Combust. Inst.* **2002**, *29*, 1775–1783.

39. Law, C.K.; Jomaas, G.; Bechtold, J.K. Cellular instabilities of expanding hydrogen/propane spherical flames at elevated pressures: Theory and experiment. *Proc. Combust. Inst.* **2005**, *30*, 159–167.

40. Jomaas, G.; Law, C.K.; Bechtold, J.K. On transition to cellularity in expanding spherical flames. *J. Fluid Mech.* **2007**, *583*, 1–26.

41. Hu, E.J.; Huang, Z.H.; He, J.J.; Zheng, J.J.; Miao, H.J. Measurements of laminar burning velocities and onset of cellular instabilities of methane-hydrogen-air flames at elevated pressures and temperatures. *Int. J. Hydrog. Energy* **2009**, *34*, 5574–5584.